

# Improving the hierarchy sensitivity of ICAL using neural network

---

**Ali Ajmi,<sup>1</sup> Abhish Dev,<sup>2</sup> Mohammad Nizam,<sup>1</sup> Nitish Nayak,<sup>2</sup> and S. Uma Sankar<sup>2</sup>**

<sup>1</sup>*Homi Bhabha National Institute, Anushaktinagar, Mumbai 400 094, India*

<sup>2</sup>*Department of Physics, Indian Institute of Technology Bombay, Mumbai 400 076, India*

*E-mail:* [aliajmi@tifr.res.in](mailto:aliajmi@tifr.res.in), [abhishdev92@gmail.com](mailto:abhishdev92@gmail.com),  
[mnizami132@gmail.com](mailto:mnizami132@gmail.com), [felarof.nayak@gmail.com](mailto:felarof.nayak@gmail.com), [uma@phy.iitb.ac.in](mailto:uma@phy.iitb.ac.in)

**ABSTRACT:** Atmospheric neutrino experiments can determine the neutrino mass hierarchy for any value of  $\delta_{CP}$ . The Iron Calorimeter (ICAL) detector at the India-based Neutrino Observatory can distinguish between the charged current interactions of  $\nu_\mu$  and  $\bar{\nu}_\mu$  by determining the charge of the produced muon. Hence it is particularly well suited to determine the hierarchy. The hierarchy signature is more prominent in neutrinos with energy of a few GeV and with pathlength of a few thousand kilometers, *i.e.* neutrinos whose direction is not close to horizontal. We use adaptive neural networks to identify such events with good efficiency and good purity. The hierarchy sensitivity, calculated from these selected events, reaches a  $3\sigma$  level, with a  $\Delta\chi^2$  of 9.

---

## Contents

<b>1</b>	<b>Introduction</b>	<b>1</b>
<b>2</b>	<b>INO and ICAL</b>	<b>4</b>
<b>3</b>	<b>Effective Selection Parameters</b>	<b>6</b>
3.1	Hits	6
3.2	Layers	7
3.3	Maximum horizontal spread of an event (maxdist)	7
3.4	Singlets	8
3.5	Triplets	8
3.6	Summarizing the effects of the selection parameters	9
<b>4</b>	<b>Choice of the analysis tool</b>	<b>10</b>
<b>5</b>	<b>Calculation of Mass Hierarchy <math>&lt; \Delta\chi^2 &gt;</math></b>	<b>11</b>
<b>6</b>	<b>Discussion</b>	<b>14</b>
<b>7</b>	<b>Acknowledgement</b>	<b>15</b>

---

## 1 Introduction

Neutrino oscillations provide us with the first glimpse of physics beyond the standard model. They explain the observed deficits in the solar and the atmospheric neutrino fluxes. The mass-squared differences needed to solve the solar neutrino problem [1] and the atmospheric neutrino problem [2] are widely different. Hence at least three neutrino mass eigenstates are required. This requirement fits nicely with the picture of three active neutrino flavours, established by the invisible decay width of  $Z^0$  boson [3]. The three flavours mix to form three non-degenerate mass eigenstates with masses  $m_1, m_2$  and  $m_3$ . We get two independent mass-squared differences  $\Delta m_{21}^2 = m_2^2 - m_1^2 = \Delta m_{\text{solar}}^2$  and  $\Delta m_{31}^2 = m_3^2 - m_1^2 = \Delta m_{\text{atm}}^2$ . Solar and atmospheric neutrino data indicate that  $\Delta m_{\text{solar}}^2 \sim 0.03 \Delta m_{\text{atm}}^2$ . Hence the third mass-squared difference  $\Delta m_{32}^2 = \Delta m_{31}^2 - \Delta m_{21}^2$  is approximately equal to  $\Delta m_{31}^2$ . The energy dependence of the solar neutrino survival probability requires  $\Delta m_{21}^2$  to be positive but there is no experimental information on  $\Delta m_{31}^2$ . Thus two very different patterns of neutrino masses are allowed:  $m_1 < m_2 < m_3$  called normal hierarchy (NH) and  $m_3 < m_1 < m_2$  called the inverted hierarchy (IH).

The unitary mixing matrix, relating the flavour eigenstates to the mass eigenstates, is parameterized by three angles  $\theta_{12}, \theta_{13}$  and  $\theta_{23}$  and one CP violating phase  $\delta_{CP}$ . In the three flavour oscillation framework, it was shown that the solar neutrino survival probability

depends on the mixing angles  $\theta_{12}$  and  $\theta_{13}$  and the atmospheric  $\nu_\mu$  survival probability depends on  $\theta_{13}$  and  $\theta_{23}$  [4, 5]. CHOOZ reactor neutrino experiment set a strong upper limit on  $\theta_{13}$  of  $\sin^2 2\theta_{13} \leq 0.1$  [6, 7]. In the limit of  $\theta_{13} \rightarrow 0$ , the solar neutrino oscillations become effective two flavour oscillations, controlled by  $\Delta m_{21}^2$  and  $\theta_{12}$ . Similarly the atmospheric neutrino oscillations are also effective two flavour oscillations, controlled by  $\Delta m_{31}^2$  and  $\theta_{23}$ . A systematic program of experiments with both natural [8–11] and man made sources [12–18] have led to a wealth of data on neutrino oscillation parameters. A three flavour oscillation fit to all the data gives the following values for these parameters, as in table 1.

$\nu$ -oscillation parameters	Best fit values	$3\sigma$ -range
$\Delta m_{21}^2$ in $10^{-5}\text{eV}^2$	7.60	7.11-8.18
$\Delta m_{31}^2$ (NH) in $10^{-3}\text{eV}^2$	2.48	2.30-2.65
$\Delta m_{31}^2$ (IH) in $10^{-3}\text{eV}^2$	2.38	2.20-2.54
$\sin^2 \theta_{12}$	0.323	0.278-0.375
$\sin^2 \theta_{23}$ (NH)	0.567	0.392-0.643
$\sin^2 \theta_{23}$ (IH)	0.573	0.403-0.640
$\sin^2 \theta_{13}$ (NH)	0.0234	0.0177-0.0294
$\sin^2 \theta_{13}$ (IH)	0.0240	0.0183-0.0297
$\delta_{\text{CP}}/\pi$ (NH)	1.34	0.0-2.0
$\delta_{\text{CP}}/\pi$ (IH)	1.48	0.0-2.0

**Table 1.** Best fit results and the  $3\sigma$ -range of the global  $3\nu$  oscillations, as from the reference [19]

The following questions still remain unanswered in the neutrino oscillation studies:

- What is the pattern of neutrino masses? Is the true hierarchy normal or inverted?
- What is the octant of the angle  $\theta_{23}$ ? Is it  $< 45^\circ$  or  $> 45^\circ$ ?
- Most importantly, is there CP violation in the neutrino sector?

A number of experiments are currently running [17, 18, 20] or being planned [21–26] to address these issues. Among the current experiments, NO $\nu$ A can determine the hierarchy for the following two favorable combinations: (i) The hierarchy is normal and  $\delta_{\text{CP}}$  is in the lower half-plane or (ii) The hierarchy is inverted and  $\delta_{\text{CP}}$  is in the upper half-plane. If nature chooses one of the other two combinations, then NO $\nu$ A has no hierarchy sensitivity [27, 28]. Present data shows a slight preference for normal hierarchy and  $\delta_{\text{CP}}$  in the lower half-plane [17, 29].

When a neutrino passes through a medium, its propagation gets modified due to the coherent forward scattering. All three flavours undergo this scattering due to neutral current (NC) interactions whereas only  $\nu_e$  has an additional scattering amplitude due to charged current (CC) scattering off electrons [30, 31]. The scattering amplitudes give rise to potential terms in the evolution equation. Since the NC interactions of all flavours are identical, the NC potential term does not lead to any modification of the oscillation probabilities. The CC potential term can lead to observable changes in the oscillation and

survival probabilities. For the muon neutrino survival probability,  $P_{\mu\mu}$ , a large change is possible only if  $\Delta m_{31}^2$  is positive, which corresponds to normal hierarchy (NH). For  $\Delta m_{31}^2$  negative, called inverted hierarchy (IH), the change in  $P_{\mu\mu}$  is negligible. For anti-neutrino the situation is reversed. The changes in the muon neutrino (or anti-neutrino) survival probability are significant when the following two conditions are satisfied [32]:

$$\Delta m_{31}^2 \cos 2\theta_{13} \sim \pm 2EV_{CC}, \quad (1.1)$$

$$\sin^2 \left( 1.27 \frac{\Delta m_{31}^2 \sin 2\theta_{13} L}{E} \right) \sim 1, \quad (1.2)$$

where  $E$  is the energy of the neutrino,  $V_{CC}$  is the potential due to CC scattering and  $L$  is the pathlength of the neutrino. The Wolfenstein matter term  $A = 2EV_{CC}$  (in  $\text{eV}^2$ ) is given by  $0.76 \times 10^{-4} \rho$  (in g/cc)  $E$  (in GeV), where  $\rho$  is the density of the matter through which the neutrino propagates. For  $\Delta m_{31}^2 \approx 2.5 \times 10^{-3} \text{ eV}^2$ , eq. (1.1) is satisfied for  $\rho E \approx 33$ . For the density 5 gm/cc of earth's mantle, the corresponding energy is  $E \approx 7$  GeV. Substituting this in eq. (1.2), we obtain a pathlength  $L$  of the order of a few thousand km. A large majority of upgoing atmospheric neutrinos pass only through earth's mantle hence the conditions mentioned above are the most relevant. Thus, we find that there is a broad range of energies around 7 GeV and a broad range of pathlengths of a few thousand kilometers for which there is an observable change in the muon neutrino survival probability [32]. However, these changes can be measured and hierarchy can be determined only if the detector has good energy and direction resolutions [33].

The plots of the muon neutrino survival probability  $P_{\mu\mu}$  for atmospheric neutrinos, as a function of neutrino energy, are shown in figure 1 for various different values of  $\cos \theta_z$ , where  $\theta_z$  is the zenith angle.

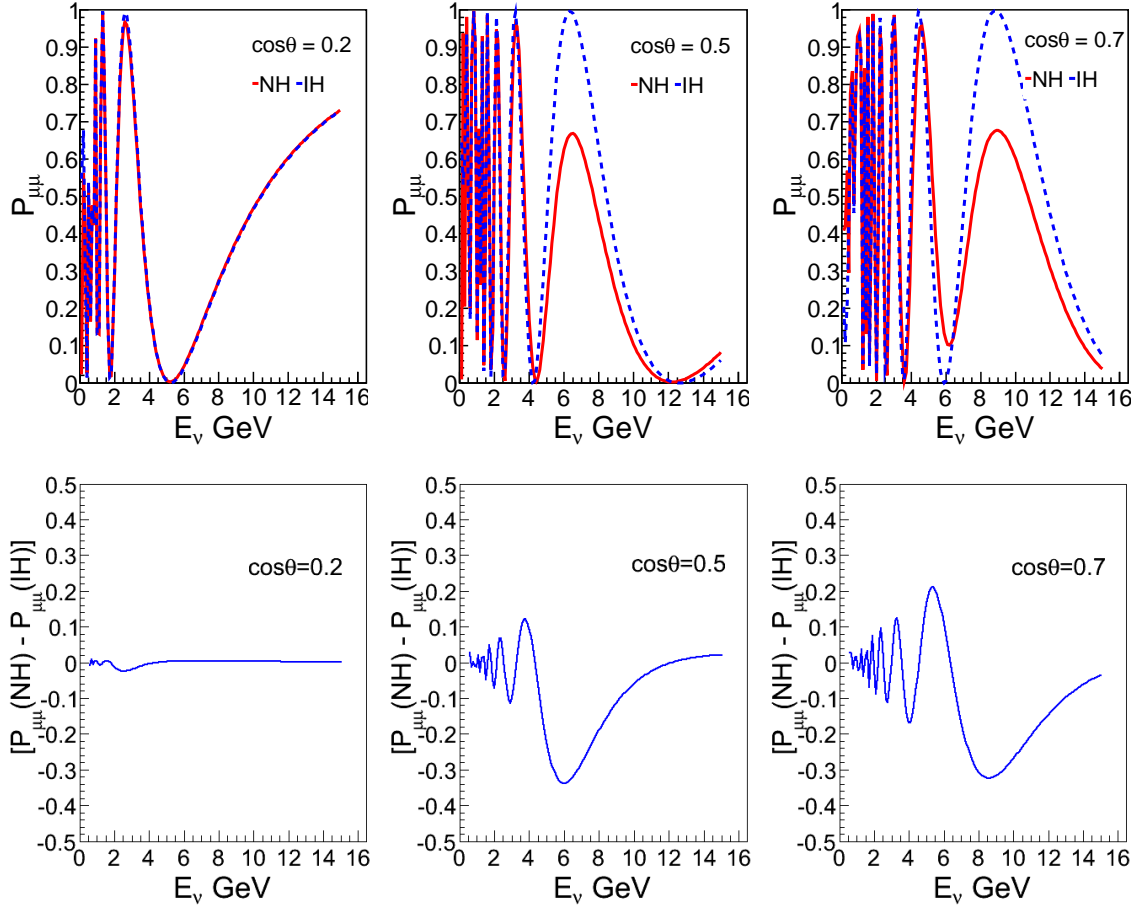


**Figure 1.** Oscillation probability plot  $P_{\mu\mu}$  for neutrinos at different zenith angles for either hierarchies (top panel). Difference between the values of  $P_{\mu\mu}$  in the NH and the IH conditions (bottom panel).

From these plots, we note that the signature for the neutrino mass hierarchy is most prominent in the energy range  $E_\nu > 4$  GeV and for  $\cos\theta_z > 0.5$ . Hence, for the purpose of hierarchy determination,  $\nu_\mu$  CC events in the *vertical cone* (i.e. with  $|\cos\theta_z| > 0.5$ ) with  $E_\nu > 4$  GeV should be considered as the signal events and all other events should be termed background. It is imperative to develop a procedure by which it is possible to select the signal events with high efficiency and purity. In this report, we develop such a procedure based on artificial neural network.

## 2 INO and ICAL

India-based Neutrino Observatory (INO) [21] is an upcoming experimental facility which can house a number of experiments requiring low cosmic ray backgrounds. A major component of the experimental program at INO is the magnetised Iron Calorimeter (ICAL) neutrino detector. It will study neutrino interactions of various types, with the atmospheric

neutrinos as the source. ICAL will be constructed in 3 modules, each of which contains 151 horizontal iron layers. The iron layers are 5.6 cm thick and they are interspersed with resistive plate chambers (RPCs) [34–36]. The total mass of the detector is made very large (more than 50 kilotons) to obtain a large sample of neutrino interaction. The area of each RPC is approximately  $2\text{m} \times 2\text{m}$  and the total number of RPCs in the detector is  $\sim 30,000$ .

When a neutrino interacts with an iron nucleus, it produces a set of charged particles. These charged particles pass through one or more RPCs, depending on the type of the particle and its energy. Whenever a charged particle passes through an RPC, it produces a hit. These hits are our primary observables. The layer number of RPC gives the z-coordinate of the hit. The x and y-coordinates are given by the copper-strips of the pick-up panels which are orthogonally oriented at the top and the bottom of the RPCs [37].

ICAL has a good ability to identify muon tracks, from the pattern of hits in successive layers, and determine the energy and the direction of the muons with good precision [38]. In the present case, our **signal** events are  $\nu_\mu\text{CC}$  events in the energy range of approx. 4-10 GeV, which are in the vertical cone. These events are expected to have long muon tracks passing through many layers. The background events come from sources: (a) low energy  $\nu_\mu\text{CC}$  interactions, (b)  $\nu_\mu\text{CC}$  interactions where neutrino direction is close to the horizontal, (c)  $\nu_e\text{CC}$  events and a small number of  $\nu_\tau\text{CC}$  events and finally (d) NC events. A large number of these background events do not give clear muon tracks. We aim to select a set of events which is highly rich in signal events. These events will have long muon tracks which can be recognized in a straight forward manner. We will utilize this fact to design criteria to separate the signal events from the background.

We exploit the energy and the direction information of the neutrinos given to us by Nuance, in order to devise/develop the selection criteria. The selection criteria, whose developement is described in detail in the next section, depend only on the visible characteristics of the  $\nu$ -events in the detector, i.e. the output parameters given by GEANT4 simulation. The neural network is trained with a selected set of events. This trained network is then applied on any random set of events. It assigns a probability to the event, denoting how close it is to a perfect signal event. The signal-like events are finally chosen based on this value. The choice of the cut is such that the signal selection efficiency and the signal purity are significantly high.

In the previous section, we argued that events with  $E_\nu > 4\text{ GeV}$  and  $\cos\theta_z > 0.5$  have the best hierarchy sensitivity. However, neutrinos over a very broad range of energy and over the full zenith angle range interact in the ICAL and produce observable events. Our job here is to develop a procedure to distinguish between the events with good hierarchy sensitivity and those without. Hence neutrino events over the full detectable range of energy must be simulated. Five different sets of data, each equivalent to 500 years of ICAL run, are generated using NUANCE in the energy range  $E_\nu = \{0.1, 100\}\text{GeV}$ . Each set consists of all types of interactions of all three neutrino flavours. The first set is generated with the assumption of no neutrino oscillations (NOOSC). The next three sets are generated assuming neutrino oscillations with normal hierarchy, with 3 different seeds. The final set is generated assuming neutrino oscillations with inverted hierarchy. The generated events are then propagated in ICAL using a Geant4 simulation of the detector. The pattern of hits

thus generated are used to first identify the muon track and then reconstruct its energy  $E_\mu$  and the cosine of its zenith angle  $\cos \theta_\mu$  [39]. In computing the oscillation probabilities, the following values of neutrino parameters were used:  $\Delta m_{21}^2 = 7.5 \times 10^{-5} \text{ eV}^2$ ,  $|\Delta m_{eff}|^2 = 2.47 \times 10^{-3} \text{ eV}^2$  (i.e.  $\Delta m_{31}^2(\text{NH}) = 2.51 \times 10^{-3} \text{ eV}^2$ ,  $\Delta m_{31}^2(\text{IH}) = -2.43 \times 10^{-3} \text{ eV}^2$ ),  $\sin^2 \theta_{12} = 0.31$ ,  $\sin^2 2\theta_{13} = 0.09$ ,  $\sin^2 \theta_{23} = 0.5$  and  $\delta_{CP} = 0$ .

### 3 Effective Selection Parameters

We first select only those events with hits in more than five layers ( $L > 5$ ). This lower limit on the number of layers is chosen to optimize the reconstruction efficiency of the muon tracks [40]. This cut also has the advantage of eliminating most of the background due to the non- $\nu_\mu$ CC events. About 90% of the events selected after this cut are  $\nu_\mu$ CC events [41]. We want the neural network to select signal events with high efficiency and good purity. We need to choose appropriate input variables for the neural network to achieve this aim. We consider a number of such variables and study their ability to distinguish between signal and background among the  $\nu_\mu$ CC events passing the  $L > 5$  cut. For this study, we divide these events into four subsets based on the neutrino energy and direction, using the information from the event generator.

1. Signal events:  $E_\nu$ : 4-100 GeV and  $|\cos \theta_z| > 0.5$ ,
2. High energy horizontal events:  $E_\nu$ : 4-100 GeV and  $|\cos \theta_z| \leq 0.5$ ,
3. Low energy vertical events:  $E_\nu$ : 0.1-4 GeV and  $|\cos \theta_z| > 0.5$ ,
4. Low energy horizontal events:  $E_\nu$ : 0.1-4 GeV and  $|\cos \theta_z| \leq 0.5$ .

We have checked that these variables discriminate against non- $\nu_\mu$ CC background very effectively.

#### 3.1 Hits

Low energy neutrino events give less number of hits compared to the high energy events. Hence, the number of hits is a measure of the energy of the neutrino as illustrated in figure (2). This variable is quite effective in distinguishing high energy events from low energy events but not for distinguishing vertical events from horizontal events.

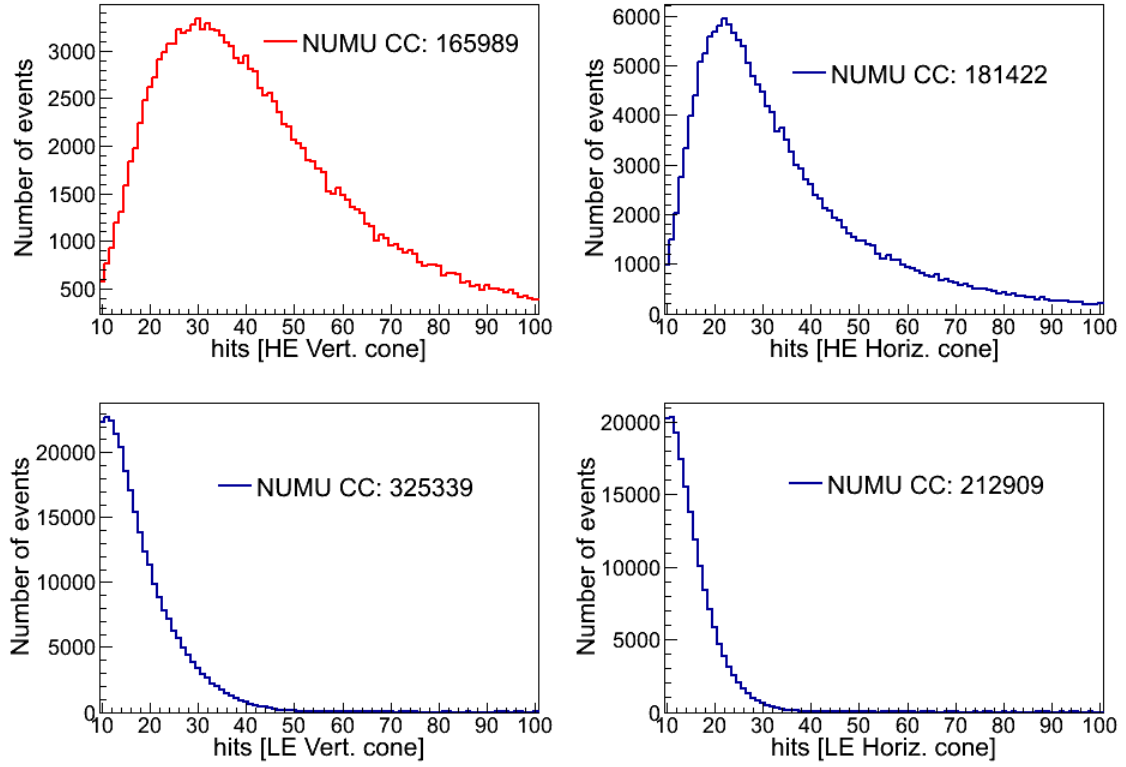


**Figure 2.** Hits Distributions for  $\nu_\mu$  CC events with  $L>5$  for the NOOSC dataset. The top left plot shows the distribution for the signal events (red).

Figure 2 shows that the signal-like events (top-left) give more hits than the low energy neutrino events (bottom row). The high energy horizontal events too give comparatively lower number of hits, if closely observed. This is due to the fact that the particles effectively travel through larger lengths of iron in the horizontal direction.

### 3.2 Layers

This parameter refers to the number of layers in ICAL, which has received one or more hits in an event. The high energy vertical neutrino events give hits in more number of layers than the low energy/horizontal events. So, the vertical  $\nu_\mu$  CC events containing high energy muon tracks give hits in a larger number of layers than the other event types.

### 3.3 Maximum horizontal spread of an event (maxdist)

The energetic but near horizontal muons have a larger spread on the horizontal plane than the vertical (or near-vertical) events. The horizontal spread between a pair of hits is given by  $D = \sqrt{((x_2 - x_1)^2 + (y_2 - y_1)^2)}$ . We calculate  $D$  for every pair of hits in an event and define its maxdist to be the maximum value of  $D$  [41]. The maxdist is quite large in case of high energy horizontal events and is moderate for the other three types of events, as can be seen in figure 3.



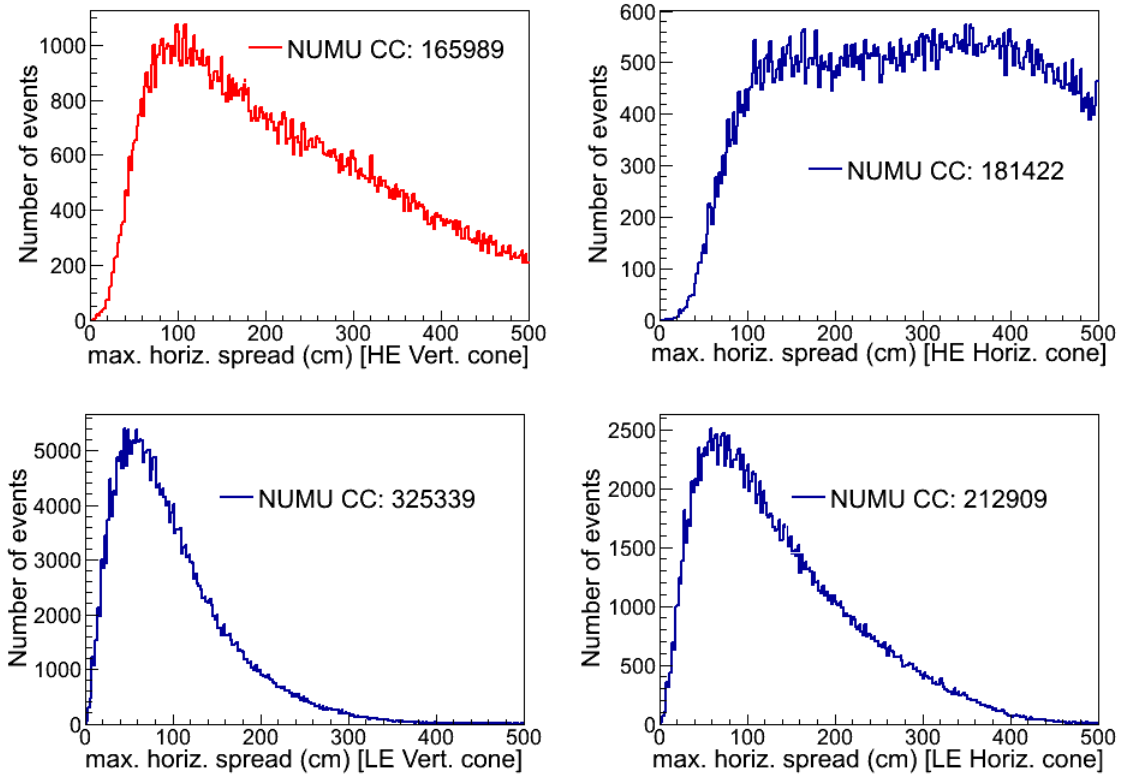


**Figure 3.** Maxdist distributions for  $\nu_\mu$  CC events with  $L > 5$  for the NOOSC dataset. The top left plot shows the distribution for the signal events (red).

### 3.4 Singlets

A high energy vertical muon passes through a number of layers. Any hadrons produced in the same event will pass through a much smaller number of layers. Therefore, in a high energy vertical event, there will be only hits due to the muon tracks after the initial few layers. For these later layers, we expect one or two hits in a layer. Almost all signal events must contain one or more layers with a single hit. The passage of a muon through an RPC can produce a hit in a single strip or hits in two adjacent strips. Therefore, we define a layer with a single hit to be one where there is only one hit or one where there are two hits in adjacent strips. *Singlets* is the number of layers in an event that contain a single hit. A signal event is expected to contain more singlets than the low energy or the horizontal  $\nu_\mu$  CC events.

### 3.5 Triplets

This is an extension of the previous parameter. *Triplets* is the number of 3 consecutive layers with single hits in an event. A signal event with a long muon track is expected to contain at least one such triplet. This variable gives more weightage to events with longer muon track with many consecutive single hit layers. For example, an event with five consecutive single hit layers has *three* triplets.

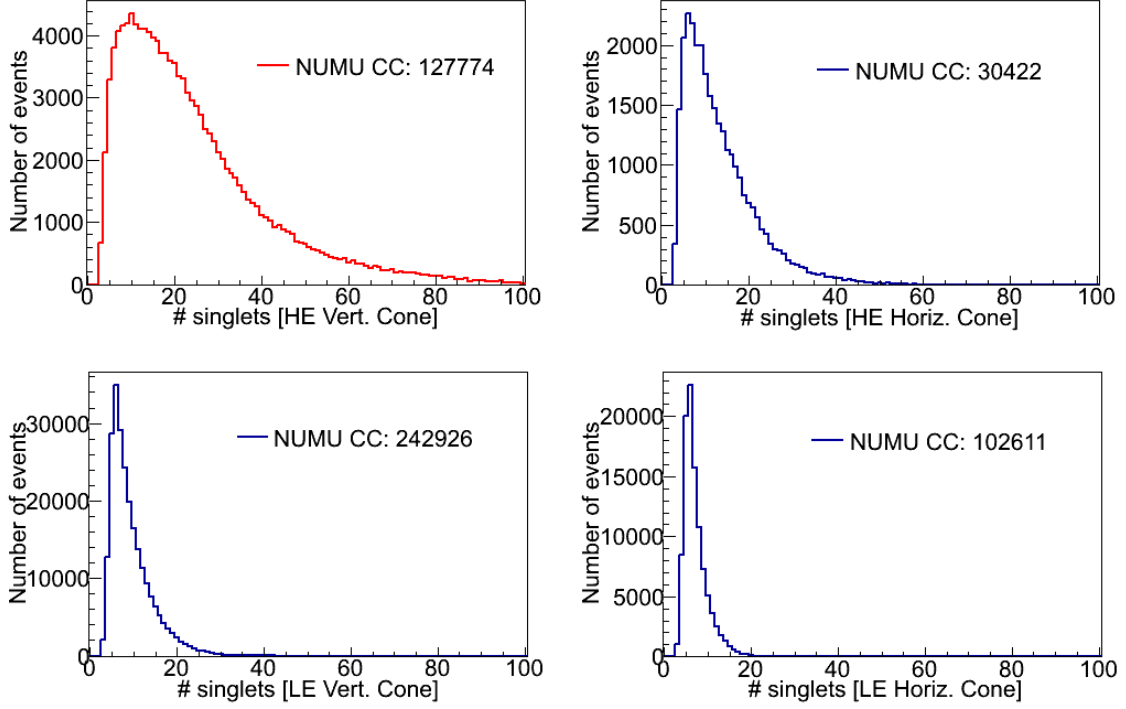


**Figure 4.** Distribution of the single-hit layers in the  $\nu_\mu$ CC events ( $L > 5$ ), combined with  $\text{maxdist}/\text{layers} \leq 10$  and  $\# \text{ possible triplets} > 0$ , for the NOOSC dataset. The top left plot shows the distribution for the signal events (red).

Figure 4 shows an example of the efficacy of the listed parameters in selecting the signal events and in discriminating against the background events. In this figure, the singlet distribution is plotted for those satisfying the simple cuts: number of triplets non-zero and the ratio  $\text{maxdist}/\text{layers} \leq 10$ . These distributions show that a cut of number of singlets  $\geq 10$  retains most of the signal events while rejecting a very large fraction of background events.

### 3.6 Summarizing the effects of the selection parameters

The above subsections all lead to the following inference:

- Hits or layers can distinguish the low energy from the high energy range  $\nu$  events.
- Maxdist distinguishes the horizontal high energy events from the rest.
- The high energy vertical  $\nu_\mu$ CC events contain significantly larger number of singlets than the low energy/ horizontal events.
- The hits-pattern across the layers in case of the high energy vertical  $\nu_\mu$ CC events form more number of triplets than the the other three categories of  $\nu_\mu$ CC events considered.

## 4 Choice of the analysis tool

The parameters discussed in the above section indicate a reliable way to select our required signal events. A selection based on neural network techniques, with these parameters as inputs, can select the signal events efficiently. So, we employ tools for multi variate analysis (TMVA), a package integrated in ROOT, for our signal selection [42].

There are a number of applicable methods that involve multivariate analysis. Methods like BDT (Boosted Decision Trees), MLP (Multi-Layer Perceptron), LikelihoodPCA (Likelihood method using the input variables after Principal Component Analysis), HMatrix (method involving the inverse of the covariance matrix; a covariance matrix is devised based on the input variables for both, the signal and the background), and TMlpANN (a ROOT [43] class TMultiLayerPerceptron) are all competitive. We did a preliminary analysis using each of these methods and compared the results. It was found that the event sample selected by TMlpANN had the best signal efficiency and purity. In addition, the time taken for the method to learn the discrimination and apply it to an event sample was also the least. In view of this the analysis was done using TMlpANN. Detailed optimization has shown that the stochastic learning method with three nodal steps and three hundred iterations gave the best performance. We applied the method on a training set of 20000 events with the signal to background ratio being the same as that in the actual data. The size of the training set was chosen after detailed optimization. The training and testing sets, post optimization, were taken from the NOOSC data set.

During the training, the selection parameters, discussed in section 3, are given as inputs to the adaptive neural network (ANN). The ANN combines these inputs in various weights to perform a number of intermediate calculations. Over a number of iterations, the trained ANN optimizes the weights and finally learns to assign a number to an event. This number is the probability of the event being a signal event. After the training, the ANN is fed the events from the NH data sets and the IH data set. The signal events are selected from each data set based on a cut on the probability assigned by the ANN (called ANNcut).

In our initial analysis, we defined the signal events to be  $\nu_\mu$ CC events with  $E_\nu > 4$  GeV and  $|\cos \theta_z| > 0.5$ . But some hierarchy discrimination is present in events with lower energy and smaller  $|\cos \theta_z|$ . So we systematically lowered the minimum values of  $E_\nu$  and  $\cos \theta_z$  and found that the best hierarchy discrimination sensitivity is obtained with  $E_\nu > 2$  GeV and  $|\cos \theta_z| > 0.2$ , as shown in figure 5. The details of the calculation of the hierarchy discrimination sensitivity are given in the next section.

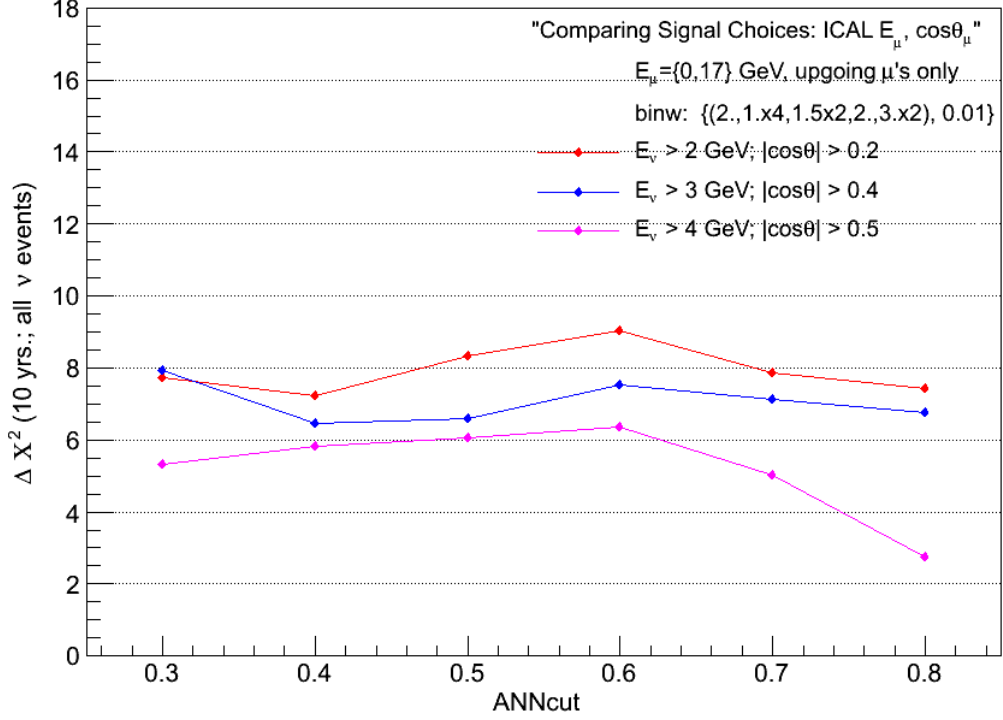


**Figure 5.** Hierarchy discrimination sensitivity for different signal definitions

## 5 Calculation of Mass Hierarchy $\langle \Delta\chi^2 \rangle$

Our redefined signal consists of the  $\nu_\mu$ CC events with  $E_\nu = \{2,100\}$ GeV and  $|\cos\theta| > 0.2$ . Therefore, the background comprises of all the rest of the  $\nu_\mu$ CC events as well as all non- $\nu_\mu$ CC events (i.e., all NCs,  $\nu_e$ CC and  $\nu_\tau$ CC). If we impose the cut  $L > 5$  on the 500 year dataset with IH oscillations, the remaining data sample has the composition shown in table 2. The numbers for NH oscillations are similar.

Total signal events	Total bkg. events
$\sim 350,000$	$\sim 400,000$

**Table 2.** Counts of the events after a cut of  $L_{\text{layers}} > 5$ , in a 500 years data sample.

For the selected signal-like events, the muon energy  $E_\mu$  and its direction  $\cos\theta_\mu$  are reconstructed. The events are sorted into bins of the reconstructed  $E_\mu$  and  $\cos\theta_\mu$ . A better angular resolution leads to a better hierarchy discrimination in atmospheric neutrino experiments [33, 44]. Hence the bin width in  $\cos\theta_\mu$  needs to be as small as possible. Here it is chosen to be 0.01, which is the  $\cos\theta_\mu$  resolution of the ICAL [38]. The down going events undergo no oscillation and hence there will not be any signature of matter effect in

them. It is present only in the up going events. Hence in computing the  $\Delta\chi^2$  for hierarchy signal, we will consider only the up going events, *i.e.* events with  $\cos\theta_\mu \in [0, 1]$ . This has the advantage of eliminating the contribution of the fluctuations in the down going events to the  $\chi^2$ .

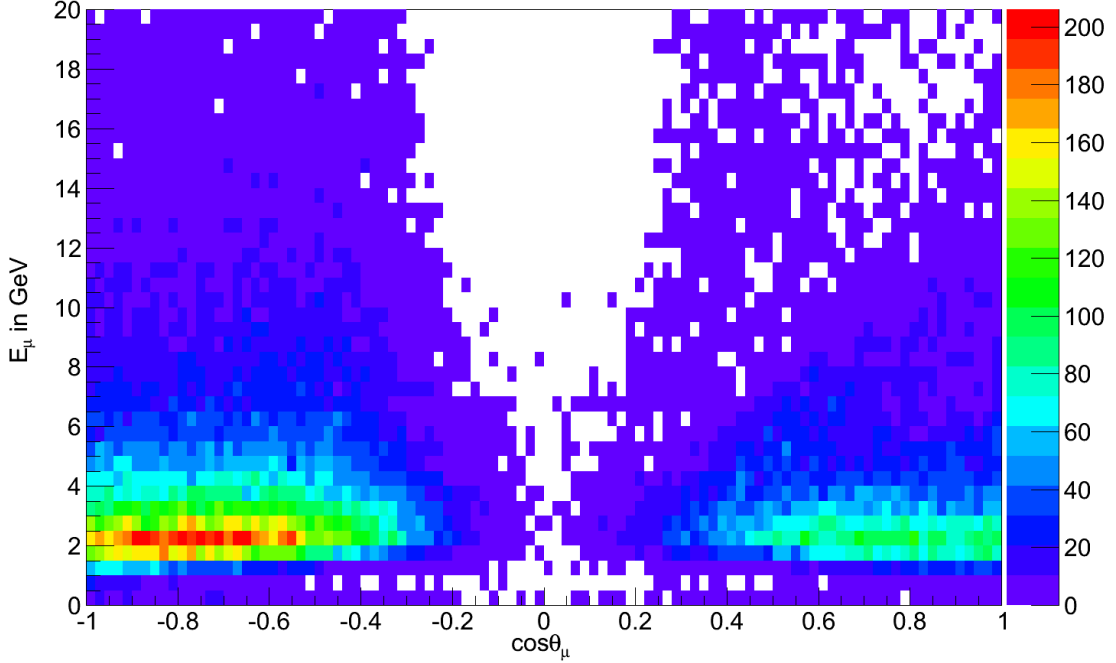


**Figure 6.** The distribution of muon energy and direction (given by NUANCE) of the events surviving the cut on the neural network probability = 0.7.

Regarding the binning in muon energy, different schemes were tested. We restricted the range of muon energies to be (0,17) GeV. Since events with very high energy muons are rather small in number, their contribution to hierarchy discrimination is very small. Also, the smaller event numbers have large fluctuations which lead to spurious contribution to hierarchy sensitivity. Therefore a binning scheme with uniform energy bins is not preferred. We have verified that the results are much better for a scheme with differential energy bins compared to a scheme with uniform energy bins. The  $L > 5$  cut as well as the selection based on ANN strongly discriminate against events with  $E_\mu < 1$  GeV. This can be seen in figure 6. Therefore, our lowest energy bin is chosen to be (0, 2) GeV, so that the number of events in this bin are substantial. We found the following 10  $E_\mu$  bins to be optimal: (0, 2), (2, 3), (3, 4), (4, 5), (5, 6), (6, 7.5), (7.5, 9), (9, 11), (11, 14) and (14, 17) GeV. The binning is done separately for  $\mu^-$  and  $\mu^+$  events. Differential binning schemes are also tried out for  $\cos\theta_\mu$ . But results of the uniform binning scheme with 0.01 bin width are always better.

For the hierarchy discrimination analysis the four data sets  $NH1, NH2, NH3$  and  $IH$

were used. Each of them was binned according to the scheme described above. From this binned data, we compute 3 values of  $\chi^2_{\text{true}}$  as  $\chi^2(NH1 - NH2)$ ,  $\chi^2(NH1 - NH3)$  and  $\chi^2(NH2 - NH3)$ , and take their average to obtain  $\langle \chi^2_{\text{true}} \rangle$ . This is expected to be twice the number of bins. We also compute 3 values of  $\chi^2_{\text{false}}$  as  $\chi^2(NH1 - IH)$ ,  $\chi^2(NH2 - IH)$  and  $\chi^2(NH3 - IH)$ , and take their average to obtain  $\langle \chi^2_{\text{false}} \rangle$ . From these we obtain  $\langle \Delta\chi^2 \rangle = \langle \chi^2_{\text{false}} \rangle - \langle \chi^2_{\text{true}} \rangle$ . We obtained a maximum  $\langle \Delta\chi^2 \rangle = 9$  (assuming a 10 year run) for an ANN probability cut of 0.6. The variation in  $\langle \Delta\chi^2 \rangle$  with the ANN probability is plotted in figure 7.

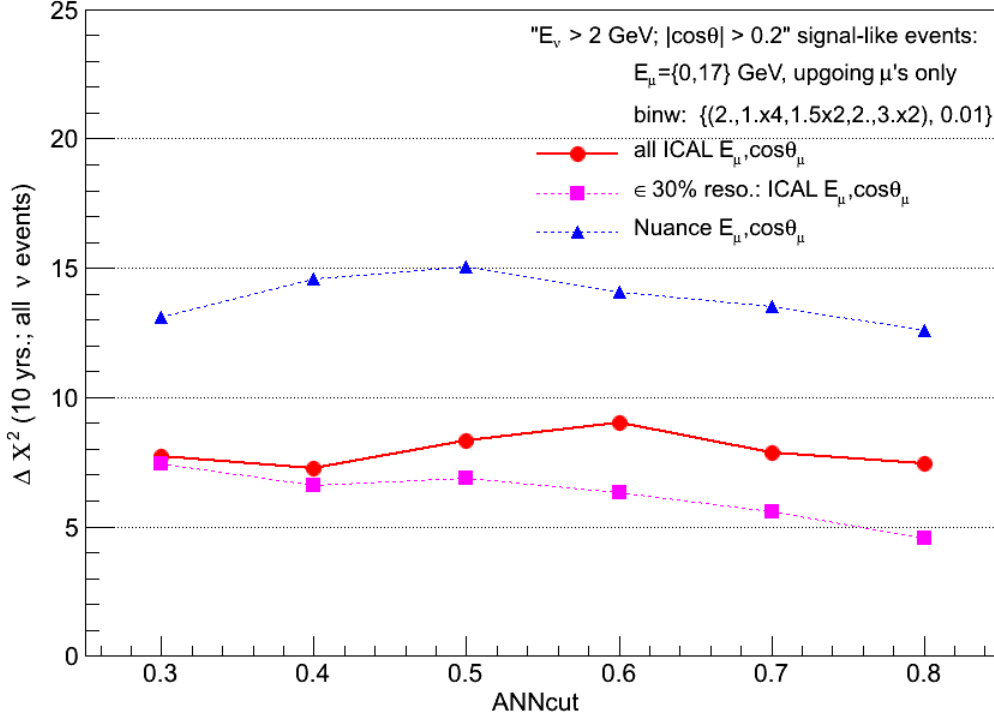


**Figure 7.** Values of  $\langle \Delta\chi^2 \rangle$  for 10 years, against varying cuts on the probability obtained from the neural network analysis, in the range  $E_\mu = \{0, 17\}$  GeV and  $\cos\theta > 0$ , using a differential binning scheme. The red circles correspond to the case where  $E_\mu$  and  $\cos\theta_\mu$  are obtained from the ICAL reconstruction code. The magenta squares correspond to the case where  $E_\mu$  is restricted to be within 30% of its Nuance value. The blue triangles show the result assuming an ideal momentum reconstruction.

Figure 7 contains two other plots which are put in for comparison. The blue curve in figure 7 shows the hierarchy discrimination of an ideal detector, which gives the exact values of  $E_\mu$  and  $\cos\theta_\mu$ . This sets the upper limit on the hierarchy discrimination of ICAL, when only  $E_\mu$  and  $\cos\theta_\mu$  are used as inputs. In addition, we considered the possibility that the fluctuations due to inefficiencies in the reconstruction are responsible for  $\langle \Delta\chi^2 \rangle$ . To rule out this possibility, we considered only those events which satisfied the following two

criteria: (i) The charge of the muon is correctly identified and (ii) The reconstructed  $E_\mu$  is within 30% of the NUANCE value. These restrictions give us a smaller event sample. The  $\langle \Delta\chi^2 \rangle$  from this subset is shown as the magenta curve in figure 7. For this restricted set, the maximum  $\langle \Delta\chi^2 \rangle = 7$ , which is close to the value of 9 obtained for the full sample. Therefore, the hierarchy discrimination we obtained comes mostly from well reconstructed events.

## 6 Discussion

We have used a neural network to identify high energy  $\nu_\mu$  CC events in the vertical direction. The neural network is able to select such events with an efficiency  $> 70\%$ . The purity of the selected samples is also  $> 70\%$ . We have binned the selected signal events in  $E_\mu$  and  $\cos\theta_\mu$  to compute the hierarchy sensitivity of ICAL. Since this sensitivity depends strongly on the angular resolution, we chose a rather fine bin width of 0.01 for  $\cos\theta_\mu$ . For binning  $E_\mu$ , we found that a scheme with differential bin widths gives a much better sensitivity. Hence we chose a set of ten bins with finer bins at lower energy and wider bins at higher energy. We also imposed an upper limit  $E_\mu \leq 17$  GeV.

From figure 7, we see that the  $\langle \Delta\chi^2 \rangle$  has only a mild dependence on ANNcut. Hence we did a brief study on the role played by the ANN in signal selection. These results are summarised in figure 8, which plots  $\langle \Delta\chi^2 \rangle$  vs. ANNcut, for uniform energy binning scheme and for differential energy binning scheme. The  $\langle \Delta\chi^2 \rangle$  for the differential scheme is always larger than the uniform scheme. In case of the uniform scheme, signal selection through ANN plays an important role and improves  $\langle \Delta\chi^2 \rangle$  from 3.5 to 8. On the other hand, the differential scheme inherently extracts the differences between the event spectra of NH and IH. For this scheme, the event selection due to ANN leads only to a small improvement in  $\langle \Delta\chi^2 \rangle$  from 7 to 9.

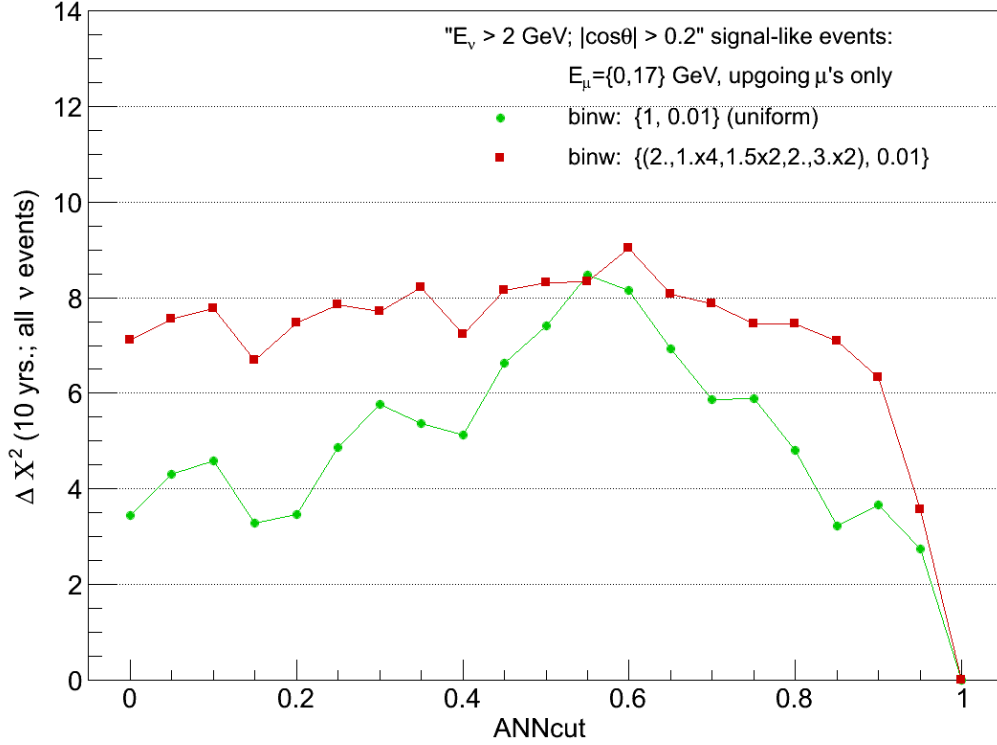


**Figure 8.** Values of  $\langle \Delta\chi^2 \rangle$  for 10 years against ANNcut, in the range  $E_\mu = \{0, 17\}$  GeV and  $\cos\theta > 0$ , using a uniform binning scheme and a differential binning scheme.

For the sample we chose, we obtained a maximum  $\langle \Delta\chi^2 \rangle = 9$ , *i.e.* a  $3\sigma$  hierarchy discrimination. We have calculated the increase in  $\langle \Delta\chi^2 \rangle$  which can happen in the case of an ideal detector. It is found that with absolute energy reconstruction, very fine direction resolution and perfect charge identification, one can obtain a  $\langle \Delta\chi^2 \rangle \sim 15$ . Therefore improvement in the muon energy reconstruction and charge identification will certainly improve the hierarchy sensitivity of ICAL.

## 7 Acknowledgement

We thank the members of the INO collaboration for all the support and cooperation we received in the course of this work. In particular, we thank Jim Libby for a discussion on the use of neural networks.

## References

- [1] J. N. Bahcall, M. Gonzalez-Garcia, and C. Pena-Garay, *Solar neutrinos before and after neutrino 2004*, *JHEP* **0408** (2004) 016, [[hep-ph/0406294](#)].
- [2] **Super-Kamiokande Collaboration** Collaboration, Y. Fukuda et al., *Evidence for oscillation of atmospheric neutrinos*, *Phys.Rev.Lett.* **81** (1998) 1562–1567, [[hep-ex/9807003](#)].



- [3] **ALEPH, DELPHI, L3, OPAL, SLD, LEP Electroweak Working Group, SLD Electroweak Group, SLD Heavy Flavour Group** Collaboration, S. Schael et al., *Precision electroweak measurements on the Z resonance*, *Phys.Rept.* **427** (2006) 257–454, [[hep-ex/0509008](#)].
- [4] T.-K. Kuo and J. T. Pantaleone, *The Solar Neutrino Problem and Three Neutrino Oscillations*, *Phys.Rev.Lett.* **57** (1986) 1805–1808.
- [5] J. T. Pantaleone, *Constraints on three neutrino mixing from atmospheric and reactor data*, *Phys.Rev.* **D49** (1994) 2152–2155, [[hep-ph/9310363](#)].
- [6] **CHOOZ** Collaboration, M. Apollonio et al., *Initial results from the CHOOZ long baseline reactor neutrino oscillation experiment*, *Phys.Lett.* **B420** (1998) 397–404, [[hep-ex/9711002](#)].
- [7] M. Narayan, G. Rajasekaran, and S. U. Sankar, *Three flavor implications of CHOOZ result*, *Phys.Rev.* **D58** (1998) 031301, [[hep-ph/9712409](#)].
- [8] **SAGE** Collaboration, J. Abdurashitov et al., *Solar neutrino flux measurements by the Soviet-American Gallium Experiment (SAGE) for half the 22 year solar cycle*, *J.Exp.Theor.Phys.* **95** (2002) 181–193, [[astro-ph/0204245](#)].
- [9] **GALLEX** Collaboration, W. Hampel et al., *GALLEX solar neutrino observations: Results for GALLEX IV*, *Phys.Lett.* **B447** (1999) 127–133.
- [10] **Super-Kamiokande** Collaboration, Y. Fukuda et al., *Measurements of the solar neutrino flux from Super-Kamiokande’s first 300 days*, *Phys.Rev.Lett.* **81** (1998) 1158–1162, [[hep-ex/9805021](#)].
- [11] **SNO** Collaboration, Q. Ahmad et al., *Measurement of the rate of  $\nu_e + d \rightarrow p + p + e^-$  interactions produced by  $^8B$  solar neutrinos at the Sudbury Neutrino Observatory*, *Phys.Rev.Lett.* **87** (2001) 071301, [[nucl-ex/0106015](#)].
- [12] **KamLAND** Collaboration, T. Araki et al., *Measurement of neutrino oscillation with KamLAND: Evidence of spectral distortion*, *Phys.Rev.Lett.* **94** (2005) 081801, [[hep-ex/0406035](#)].
- [13] **MINOS** Collaboration, D. Michael et al., *Observation of muon neutrino disappearance with the MINOS detectors and the NuMI neutrino beam*, *Phys.Rev.Lett.* **97** (2006) 191801, [[hep-ex/0607088](#)].
- [14] **Double Chooz** Collaboration, Y. Abe et al., *Indication for the disappearance of reactor electron antineutrinos in the Double Chooz experiment*, *Phys.Rev.Lett.* **108** (2012) 131801, [[arXiv:1112.6353](#)].
- [15] **Daya Bay** Collaboration, F. An et al., *Spectral measurement of electron antineutrino oscillation amplitude and frequency at Daya Bay*, *Phys.Rev.Lett.* **112** (2014) 061801, [[arXiv:1310.6732](#)].
- [16] **RENO** Collaboration, J. Ahn et al., *Observation of Reactor Electron Antineutrino Disappearance in the RENO Experiment*, *Phys.Rev.Lett.* **108** (2012) 191802, [[arXiv:1204.0626](#)].
- [17] **T2K** Collaboration, K. Abe et al., *Observation of Electron Neutrino Appearance in a Muon Neutrino Beam*, *Phys.Rev.Lett.* **112** (2014) 061802, [[arXiv:1311.4750](#)].
- [18] **T2K** Collaboration, K. Abe et al., *Precise Measurement of the Neutrino Mixing Parameter  $\theta_{23}$  from Muon Neutrino Disappearance in an Off-Axis Beam*, *Phys.Rev.Lett.* **112** (2014) 181801, [[arXiv:1403.1532](#)].

- [19] D. Forero, M. Tortola, and J. Valle, *Neutrino oscillations refitted*, *Phys.Rev.* **D90** (2014) 093006, [[arXiv:1405.7540](#)].
- [20] **NOvA** Collaboration, D. Ayres et al., *NOvA: Proposal to build a 30 kiloton off-axis detector to study  $\nu(\mu)$  —  $\bar{\nu}(e)$  oscillations in the NuMI beamline*, [hep-ex/0503053](#).
- [21] **INO Collaboration** Collaboration, M. S. Athar et al., *India-based Neutrino Observatory: Project Report. Volume I.*, 2006.
- [22] **IceCube PINGU** Collaboration, M. Aartsen et al., *Letter of Intent: The Precision IceCube Next Generation Upgrade (PINGU)*, [arXiv:1401.2046](#).
- [23] **Hyper-Kamiokande Proto-Collaboration** Collaboration, K. Abe et al., *Physics Potential of a Long Baseline Neutrino Oscillation Experiment Using J-PARC Neutrino Beam and Hyper-Kamiokande*, *PTEP* (2015) [[arXiv:1502.05199](#)].
- [24] **LBNE** Collaboration, C. Adams et al., *The Long-Baseline Neutrino Experiment: Exploring Fundamental Symmetries of the Universe*, [arXiv:1307.7335](#).
- [25] **JUNO** Collaboration, F. An et al., *Neutrino Physics with JUNO*, [arXiv:1507.05613](#).
- [26] S.-H. S. Seo, *New results from RENO and Future RENO-50*, Talk delivered at EPS-HEP 2015, Vienna, 2015.
- [27] P. Huber, M. Lindner, T. Schwetz, and W. Winter, *First hint for CP violation in neutrino oscillations from upcoming superbeam and reactor experiments*, *JHEP* **11** (2009) 044, [[arXiv:0907.1896](#)].
- [28] S. Prakash, S. K. Raut, and S. U. Sankar, *Getting the Best Out of T2K and NOvA*, *Phys. Rev.* **D86** (2012) 033012, [[arXiv:1201.6485](#)].
- [29] M. Sanchez, “Results and Prospects from the Nova experiment.” <http://nova-docdb.fnal.gov/cgi-bin/RetrieveFile?docid=13893&filename=nova-nufact-2015.pdf&version=2>, 2015.
- [30] L. Wolfenstein, *Neutrino Oscillations in Matter*, *Phys.Rev.* **D17** (1978) 2369–2374.
- [31] S. Mikheev and A. Y. Smirnov, *Resonance Amplification of Oscillations in Matter and Spectroscopy of Solar Neutrinos*, *Sov.J.Nucl.Phys.* **42** (1985) 913–917.
- [32] R. Gandhi, P. Ghoshal, S. Goswami, P. Mehta, and S. U. Sankar, *Earth matter effects at very long baselines and the neutrino mass hierarchy*, *Phys. Rev.* **D73** (2006) 053001, [[hep-ph/0411252](#)].
- [33] S. Petcov and T. Schwetz, *Determining the neutrino mass hierarchy with atmospheric neutrinos*, *Nucl.Phys.* **B740** (2006) 1–22, [[hep-ph/0511277](#)].
- [34] R. Cardarelli, G. Aielli, P. Camarri, A. Di Ciaccio, B. Liberti, et al., *Track resolution in the RPC chamber*, *Nucl.Instrum.Meth.* **A572** (2007) 170–172.
- [35] W. Riegler, C. Lippmann, and R. Veenhof, *Detector physics and simulation of resistive plate chambers*, *Nucl.Instrum.Meth.* **A500** (2003) 144–162.
- [36] C. Lippmann, *Detector Physics of Resistive Plate Chambers*. PhD thesis.
- [37] S. Bheesette and for the INO collaboration, *Development of Glass Resistive Plate Chambers for INO*, *ArXiv e-prints* (Oct., 2008) [[arXiv:0810.4693](#)].
- [38] A. Chatterjee, K. Meghna, K. Rawat, T. Thakore, V. Bhatnagar, et al., *A Simulations Study*

*of the Muon Response of the Iron Calorimeter Detector at the India-based Neutrino Observatory*, *JINST* **9** (2014) P07001, [[arXiv:1405.7243](#)].

- [39] **INO Collaboration** Collaboration, G. Majumder and A. Redij, “GEANT4 based INO-ICAL simulation code.” 2011.
- [40] K. Bhattacharya, A. K. Pal, G. Majumder, and N. K. Mondal, *Error propagation of the track model and track fitting strategy for the Iron CALorimeter detector in India-based neutrino observatory*, *Comput. Phys. Commun.* **185** (2014) 3259–3268.
- [41] A. Ajmi and S. U. Sankar, *Muonless Events in ICAL at INO*, *JINST* **10** (2015) P04006, [[arXiv:1501.03252](#)].
- [42] A. Hocker, J. Stelzer, F. Tegenfeldt, H. Voss, K. Voss, et al., *TMVA - Toolkit for Multivariate Data Analysis*, *PoS ACAT* (2007) 040, [[physics/0703039](#)].
- [43] R. Brun, F. Rademakers, and S. Panacek, *ROOT, an object oriented data analysis framework*, *Conf.Proc.* **C000917** (2000) 11–42.
- [44] R. Gandhi, P. Ghoshal, S. Goswami, P. Mehta, S. U. Sankar, et al., *Mass Hierarchy Determination via future Atmospheric Neutrino Detectors*, *Phys.Rev.* **D76** (2007) 073012, [[arXiv:0707.1723](#)].